Faraday Discussions

Accepted Manuscript

Faraday Discussions

Royal Society of Chemistry

ROYAL SOCIETY
OF CHEMISTRY

ROYAL SOCIETY
OF CHEMISTRY

www.rsc.org/faraday_d

Journal Name

ARTICLE

Trioctylphosphine as self-assembly inducer

Gunadhor S. Okram[*a], Jaiveer Singh,[b] Netram Kaurav[c] and Niranjan P. Lalla[a]

Nickel nanoparticles (NPs) of different shapes and sizes in the polydispersed as well as monodispersed forms were synthesized using trioctylphosphine (TOP), triphenylphosphine (TPP), oleylamine (OA) and their combinations as surfactants to study their self-assembly inducing capability. Randomly agglomerated polydispersed NPs were found for TPP and OA, and TPP or OA separately. However, in consolidation with the earlier report of Singh et al. *J. Mater. Chem. C* 2014, **2**, 8918, NPs formed using TOP only and combination of it with OA naturally exhibited monodispersed NPs associated with natural nanolattice formation without any other external force or surfactants demonstrating clearly the self-inducing capacity of TOP into monodispersed NPs and their self-assembled nanolattices. Fourier-transformed infra-red (FTIR) data clearly indicated the capping of these surfactants along with acetylacetonate ligands from nickel acetylacetonate precursor on the surface of the NPs. Remarkably, narrowest zeta potential (ζ) base-widths were observed for samples possessing self-assembled nanolattice compared to the broader ones for randomly agglomerated particles.

1. Introduction

The self-assembly of NPs into three-dimensional (3D) NP lattice (briefly, nanolattice) is crucial for utmost future applications in, for example, novel detector, optical, magnetic recording and electronic metamateials,[1-3] and fundamental understanding.[4,5] However, the external forces have so far been their cohesive forces[6-9] not their own as in atomic lattice for self-assembly, leading to a challenge for its genuine bulk 3D nanolattice[1-3,6-9] and hence requiring search for self-generated cohesive forces.[8,10] It is because such nanolattices possess properties superior to those of individual NPs and bulk material of the same composition. Nevertheless, we cannot appreciate them precisely unless we understand fully their significant dependence on the synthetic conditions, in addition to their dependence on surface, size, shape and hence their assembly. The fundamental reasons behind these facts are their profound sensitivities to the nascent surface dangling bonds to get reacted easily. These are quite often controlled initially with the cappant/ surfactant used for their stabilization [6,11-16]. These situations impose directly on their crystal structure and hence their fundamental properties and applications. Therefore, synthesis of nanoscale materials with desired properties is rather tricky and presents a great challenge to the materials scientists. The frequently encountered obstacle during and after the synthesis of metal NPs is the spontaneous surface oxidation, which quite often occurs even in passivated surfaces as well to a great degree to a minimum [6,10,11-16]. Therefore, appropriate choice of surfactants is very crucial. A brief report in this has been presented by Singh et al. [10]. In this, they reported the formation of strikingly dramatic natural assembly of nickel NPs into bulk 3D hexagonal close-packed (hcp) nanolattice, akin to atomic crystal lattice without external force, in the systematically tuned nickel NPs of different average particle sizes whenever TOP is one of the surfactants. Their analytical calculations using the grazing incidence X-ray diffraction (GIXRD) peaks of glass drop-casted thin film as well as in usual powder form showed clear bulk hcp nanolattice structure with remarkable c/a ratios analogous to usual atomic hcp lattice. This natural assembly approach, and insight into the design condition it was achieved, is believed to pave the way towards devising both new class of genuinely natural multicomponent metamaterials for fundamental studies and the exploration of varieties of phase characteristics for desired future hybrid devices. More details on this work shall be discussed in the present paper in relation to nanolattice formation capacity of TOP compared to other surfactants such as OA and TPP. To enable this, we have prepared different samples of nickel NPs with varying concentrations of TOP, TPP and OA, and independently for each of them.

2. Experimental

2.1 Sample preparation

Nickel NPs were prepared by the thermal decomposition method.[10] Typically 2.0 g of preheated (215℃) TPP (99%, Sigma Aldrich) was added in the already degassed (at 100 °C for 30 min.) solution of 1.002 g Ni(acac)$_2$ (95% Aldrich) and 4 ml OA (70% Aldrich). The resulting solution was further heated at 220 °C for 2.0 hour under argon atmosphere. After the completion of the reaction, the solution was then cooled down to room temperature, and centrifuged by

adding ethanol (99.9% Jiangsu Huaxi) to extract and wash the NPs. Washing was done four times. Similar procedures were followed for 4.0 g, 6.0 g, 8.0 g and 10.0 g of TPP. These samples are denoted by Ni39, Ni40, Ni41, Ni42 and Ni43, respectively (Table 1). Such procedures without preheating were followed for four samples Ni49, Ni31, Ni50 and Ni51 for 5 ml, 8 ml, 10 ml and 15 ml OA each with 10 ml TOP. Two samples Ni48 and Ni47 were prepared in 10 ml OA only, and 10 ml TOP only, by directly heating at 220 °C for 2.0 hour in argon atmosphere. All the prepared samples of nickel NPs were characterized using various techniques.

Table 1 Summary of sample preparations

Sample	Ni(acac)$_2$	Oleylamine (100 °C, 30 m)	Cappant at 215°C	Reaction Conditions
Ni31	1.002 g	8 ml	10 ml TOP	2 h, 220 °C
Ni39	1.04 g	4 ml	2 g TPP	2 h, 220 °C
Ni40	1.04 g	4 ml	4 g TPP	2 h, 220 °C
Ni41	1.04 g	4 ml	6 g TPP	2 h, 220 °C
Ni42	1.04 g	4 ml	8 g TPP	2 h, 220 °C
Ni43	1.04 g	4 ml	10 g TPP	2 h, 220 °C
Ni44	1.04 g	-	10 g TPP	2 h, 220 °C
Ni47	1.006 g	-	10 ml TOP*	2 h, 220 °C
Ni48	1.006 g	10 ml	-	2 h, 220 °C
Ni49	1.006 g	5 ml	10 ml TOP*	2 h, 220 °C
Ni50	1.006 g	10 ml	10 ml TOP*	2 h, 220 °C
Ni51	1.006 g	15 ml	10 ml TOP*	2 h, 220 °C

*At 25°C

2.2 X-ray Diffraction (XRD)

The Bruker D8 Advance X-ray diffractometer with Cu Kα radiation (0.154 nm) in the angle range 30-90° was used for laboratory method of XRD measurements of the samples in powder form; the X-rays were detected using a fast counting detector based on silicon strip technology (Bruker LynxEye detector).

2.3 High resolution laboratory GIXRD

High resolution laboratory grazing incidence X-ray diffraction (GIXRD) measurements on glass drop-casted thin films were done with Cu Kα radiation in the angle range 0.2-10° with a step size of 0.02°; the incident X-ray angle was normally fixed at 0.5° unless it is specified.

2.4 Transmission electron microscopy (TEM)

NP images and selected area electron diffraction (SAED) were recorded using transmission electron microscopy (TECNAI-20U-G^2-TWIN and TECHNAI-20-G^2) by drop-casting the well-sonicated solution of a few milligrams of NPs dispersed in about 5 ml ethanol on carbon-coated TEM grids.

2.5 Zeta potential measurements

Zeta potential measurements using a NanPlus-3 (Particulate system) were carried out after thorough sonication of the NPs dispersed in ethanol. Approximately 8 mg NPs were dispersed in 15 ml of ethanol for a typical run at 25°C. The number of repitions was three times and their mean was taken. The scattering angle was 14.6^o with sampling time of 0.4 ms, correlation channel of 512 channels and ten times accummulation time.

2.6 Fourier-transformed Infra-Red (FTIR) absorption measurements

A few micrograms of the NPs of each sample were added to a fixed quantity of pure KBr and ground it thoroughly. Then, a pellet of the uniform mixture was made for each sample. FTIR spectrum of a pure KBr pellet was subtracted from the FTIR data of each sample to obtain the corresponding FTIRs of the samples using an FTIR spectrometer (Bruker, Vertex 70).

3. Results and Discussion

3.1 Influence of triphenylphosphine

The XRD spectra for the Ni39, Ni40, Ni41, Ni42 and Ni43 samples are shown in fig. 1. It is clear that three characteristic peaks for nickel (2 θ = 44.8, 51.8, and 76.3), corresponding to Miller indices (111), (200), and (220), are observed. They reveal that the resultant particles were pure face-centred cubic (fcc) nickel. The lattice parameters were calculated as a=3.5127 Å, 3.5179 Å, 3.5142 Å, 3.5110 Å and 3.5039 Å, respectively. Further, a close look at the
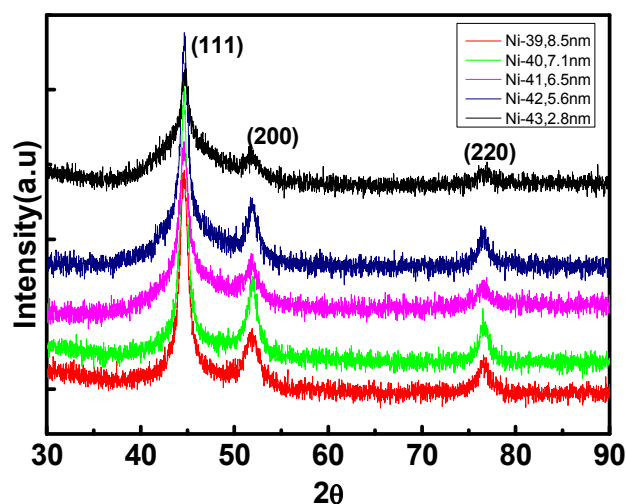
Fig. 1 X-ray diffraction patterns of nickel NPs Ni39, Ni40, Ni41, Ni42 and Ni43 samples.

peaks reveals that as the TPP concentration increases, the peak intensities gradually decreases while the full-widths at half maximum (FWHM) steadily increases suggesting that the particle size decreases with TPP concentration. Moreover, there is significant background of the XRD patterns probably due to the surfactant present on the particle surface (see in FTIR). The average particle size, determined using these peak FWHMs in the Debye-Scherer relation, showed a systematic reduction as 8.5 ± 0.5 nm, 7.4± 0.3 nm, 6.5± 0.3 nm, 5.6 ± 0.3 nm and 2.8 ± 0.2 nm, respectively.

For studying microstructure of these NPs, their typical TEM images are shown in fig. 2. It is fairly clear that the particle shape and size are quite random in their frequency of abundance (Fig. 3). Therefore, it is rather difficult to judge a reasonable average particle size of each sample as evident from figs. 2 and 3. Such particle sizes vary from 18 – 62 nm. This is in contrast to the nearly monodispersed NPs found in earlier studies wherein a combination of TOP in addition to other surfactants were reported.[6,10,11] Moreover, they generally appear to be agglomerated from smaller particles (fig. 2).

Their typical SAEDs display reasonably clear diffraction rings in all the concentrations of TPP with little spotty rings for 4 g (Ni40) and 6 g (Ni41) samples (fig. 4). Five fringe patterns with planar distances of 2.199 Å, 1.885 Å, 1.466 Å, 1.137 Å and 0.903 Å can be observed. They are related to the (111), (200), (220), (311) and (400) planes of fcc nickel. If we correlate the average particle size estimated from XRD with them, it can be understood that TEM particle size is the cumulative of region(s) in which the nickel atomic arrangements are uniform and non-uniform. The uniform
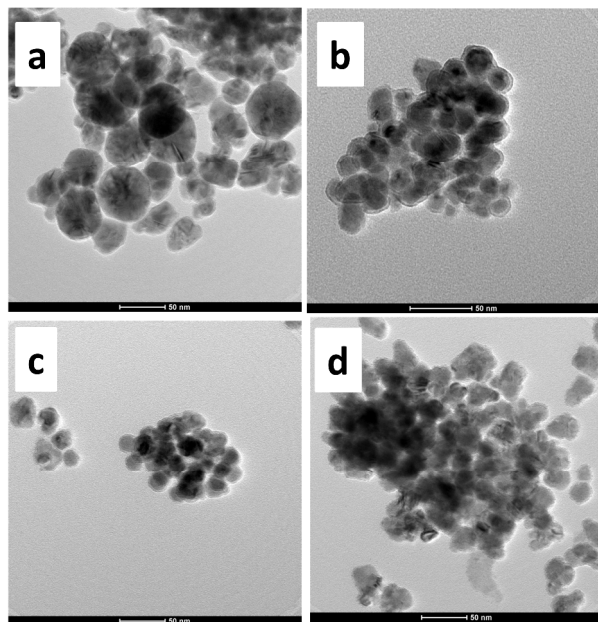
Fig. 2 TEM images of (a) 4 g TPP (Ni40), (b) 6 g TPP (Ni41), (c) 8 g TPP (Ni42) and (d) 10 g TPP (Ni43) samples. Scales: 50 nm.

region/s where the atoms are periodic is reflected in the average particle size from XRD. These uniform regions are much smaller than those of TEM image sizes. Hence, the average particle size estimated from XRD is very much smaller than those from TEM image sizes. Further, the TEM images clearly show that these particles do not exhibit systematic arrangements, as expected for a usual collection of NPs.

3.2 Influence of trioctylphosphine or oleylamine

The XRD patterns for the Ni47, Ni48, Ni49, Ni50 and Ni51 samples are shown in fig. 5. Three characteristic peaks for nickel (2θ=44.8, 51.8, and 76.3°), corresponding to Miller indices (111), (200), and (220), are observed in the case of Ni48, 10 ml OA only sample (Fig. 5a). However, only the main (111) peak near 44.8° is visible for various concentrations of OA up to 10 ml for 10 ml TOP (Ni48-Ni50). This reveals that the samples are fcc nickel. When 15 ml OA is used with 10 ml TOP, nickel NPs becomes nearly amorphous since they cannot diffract the X-rays and hence no distinct peak is observable. The FWHM for (111) reflection was used to estimate the particle size from Scherrer relation. These sizes were respectively 11.1 nm (Ni48), 0.97 nm (Ni47), 0.91 nm (Ni49) and 1.2 nm (Ni50).

The typical TEM images and SAEDs of Ni48 and Ni31, for which XRD was similar to Ni49 (not shown here), are shown in shown in figs. 6 and 7, respectively. OA only Ni48 sample show widely varied particle size in somewhat similar trend as that of TPP samples (fig. 2) but with smoother boundaries herein. Not only has that it seemed to have a Gaussian distribution of particles size (fig. 6(c)) that show the
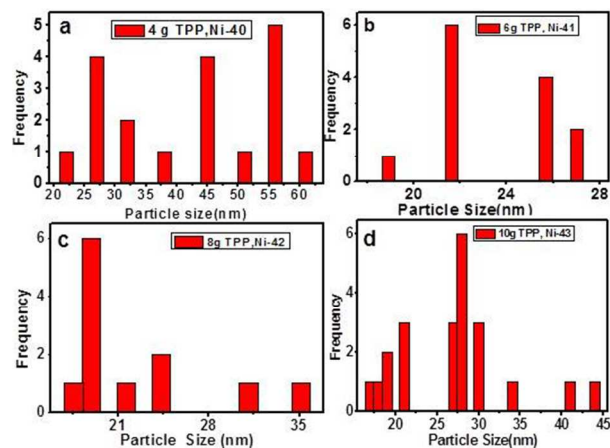
Fig. 3 Bar graphs of the particle size distributions in Ni40, Ni41, Ni42 and Ni43 TPP prepared samples indicating random size.
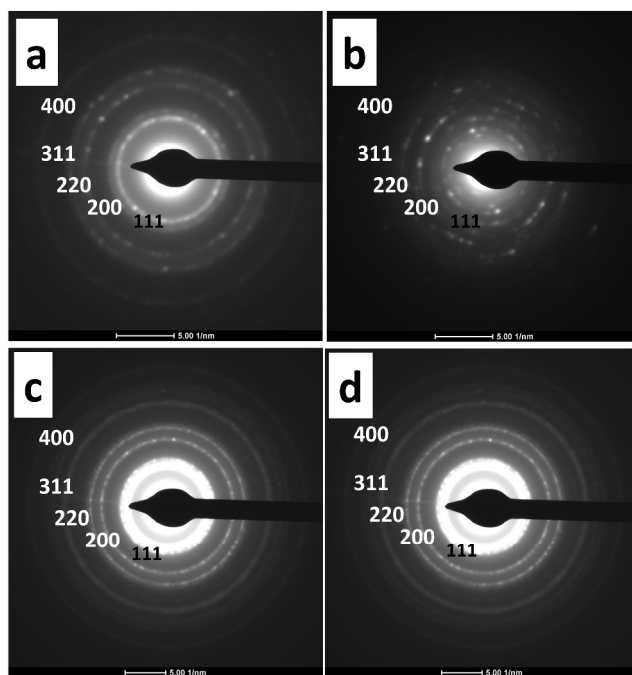
Fig. 4 Electron diffraction patterns of (a) 4 g TPP (Ni40), (b) 6 g TPP (Ni41), (c) 8 g TPP (Ni42) and (d) 10 g TPP (Ni43) samples. Scales: 5 1/nm.

maximum near 70 nm, which may be considered as the average particle size. This is so, in contrast to the Scherrer size of 11.1 nm, which indicates an average region with periodically distributed Ni atoms. The agglomerated particle size, as big as 200 nm, is seen in fig. 6(a). However, such oversized particles

are rare. They therefore show no sign of monodispersity and no sign of probable agglomerations of smaller particles without disturbing their original shape and size. Instead of this, agglomerations are in different crystal orientations thereby not forming stacking of crystal planes to form a continuous crystalline structure as a whole but in random crystal plane orientations rather than the rounded or spherical shape of the smaller NPs. This indicates that OA cannot maintain a uniform
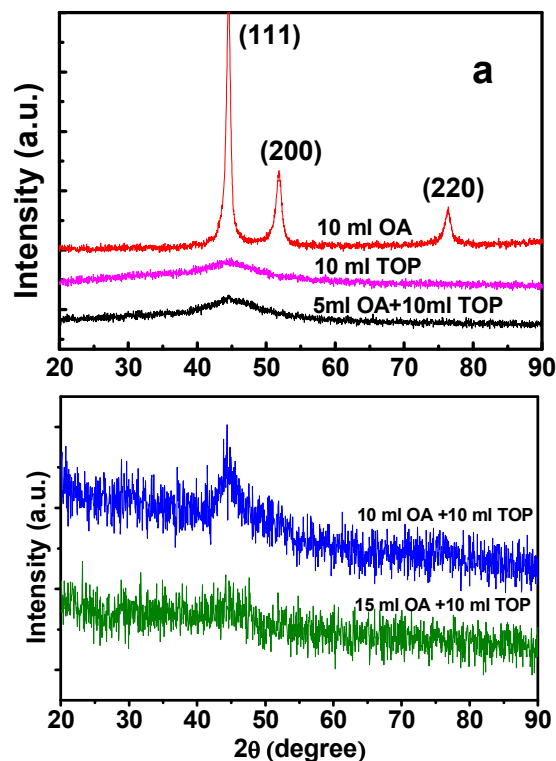
Fig. 5 X-ray diffraction patterns of nickel NPs for (a) Ni48 (for 10 ml OA only), Ni47 (for 10 ml TOP only), Ni49 (for 5 ml with 10 ml TOP) and (b) Ni50 (10 ml OA with 10 ml TOP) and Ni51 (for 15 ml OA with 10 ml TOP) samples.

particle shape and size and hence no probability of forming a nanolattice. Similar argument as those of TPP samples is considered to hold true here also for the difference in the particle size estimated from Scherrer method and TEM images. These results on the samples prepared in TPP with OA, and OA only independently clearly show that the particle size and shape are quite random, and they are agglomerated to varying sizes without showing any uniformity in the size. In contrast, samples, made in TOP and OA combined surfactants, show very uniform size and shape. Not only this, the particles form their own lattice analogous to those of atoms as demonstrated previously [10]. A typical example for Ni31 is shown in fig. 7. Clearly, the particles have uniform size (~4 nm) and shape (fig. 7 (a)- (c)). Figs. 7(a) through 7(c) represent TEM images in increasing magnifications to clearly understand their precise shape, size and their arrangements. The distinct arrangements of the particles into hexagonal closed packed (hcp) lattice into
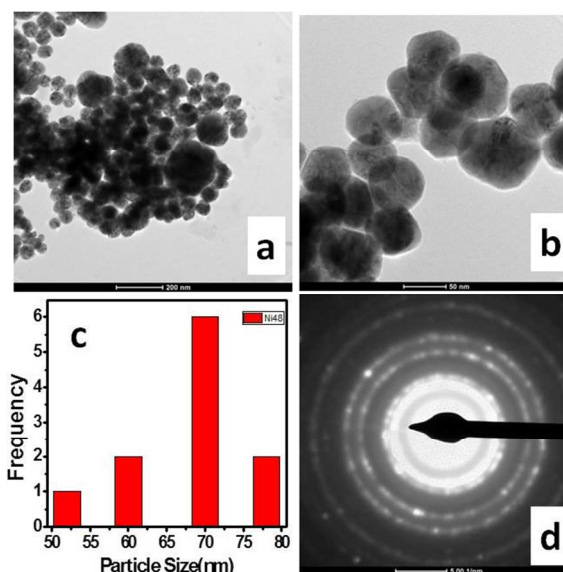
Fig. 6 (a), (b) TEM images for two magnifications, 200 nm and 50 nm scales of Ni48 sample with its (c) bar graph of the distribution of the particle size and (d) SAED.

hundreds of nanometer size NP ordering in an agglomerated large particle are evident from the image (e.g. fig. 7(a)) and also from their SAED pattern shown in fig. 7 (c), inset. Since the particle size is small (4 nm from TEM and 1.1 nm from Scherrer), they cannot provide couple of electron diffraction rings of the reflecting planes. Consequently, as in XRD (not shown), only one ring due to (111) reflection plane is seen (fig. 7(d)). This result is in contrast to that of Ni43 of 10 g TPP and 4 ml OA sample which showed three peaks in XRD (fig. 1), SAED similar to fig. 4 but having Scherrer size of 2.8 nm and 20-60 nm from TEM images (not shown). These comparisons suggest that Ni31 for TOP sample has much better, and uniform shape and size microstructure well-matched with that of atomic lattice structure (one peak in wide angle XRD), than that of Ni43. Similar line of consideration is applied to these differences for all the samples with TPP only and OA only or their combinations.

3.3 GIXRD study

Litmus test for the formation of full-fledged 3D nanolattice is expected to be confirmed without doubt through GIXRD if nanolattice happens to form since this angular region of XRD matches size of the NPs as per the Bragg law, 2d sinθ = λ, the X-ray wavelength (1.5406 Å) for n=1 i.e. the diffraction angle (sinθ) is inversely proportional to the lattice spacing (d). Therefore, how these particles exist together when they are dried as powder is interesting especially when TOP samples indicate hexagonal arrangement in TEM images and SAED pattern. For this, GIXRD measurements were performed on several of them. They are shown in fig. 8. It is clear that the samples prepared in OA and TPP together or separately i.e. Ni39, Ni40, Ni43 and Ni48 show no peak; the curves are simply steeply fallen beyond about 0.6° and smooth feature everywhere indicating that no crystal plane reflections of the

Journal Name

RSC**Publishing**
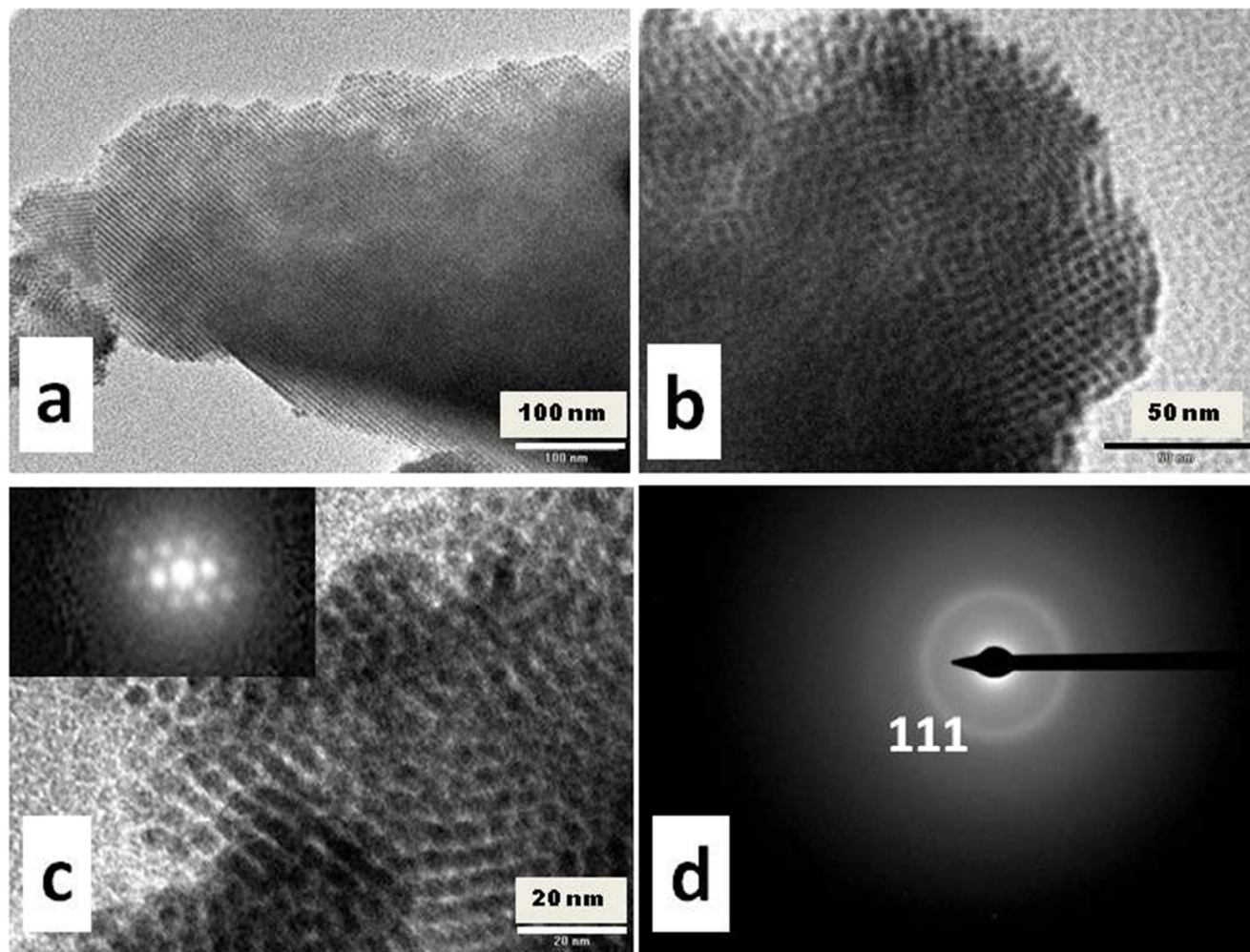
ARTICLE

Fig. 7 (a)-(c) TEM images for three magnifications with 100 nm, 50 nm and 20 nm scales of Ni31 sample with its (c) bar graph of the distribution of the particle size and (d) SAED.

NPs exist. This is in support of the random size and shape of these NPs seen in TEM (figs. 2, 3 and 6) and no evidence for formation of NP lattice planes. On the contrary, samples with TOP as surfactants viz. Ni47, Ni49, Ni50 and Ni51 show a peak each as indicated by the vertical arrows (fig. 8). Only one peak is exhibited because the incidence angle of the X-ray was 0.5°; see in ref. [10] also. These peaks are assigned to (001) reflecting plane of the hcp lattices of NPs, i.e. nanolattices are formed as crystal structure of the NPs in addition to fcc crystal structure of nickel atoms, as reported earlier [10]. Fig. 8 thus clearly indicates that TOP is the actual inducer of nanolattice, not TPP or OA. Therefore, natural nanolattice is formed only when non-ionic long- and triple-chained TOP ($C_{24}H_{51}P$) is used as surfactant, not with that of long-chain OAm ($C_{18}H_{37}N$) or phenyl group TPP ($C_{18}H_{15}P$) surfactant (fig. 9). A typical NP capped with

surfactant or impurity ions is illustrated in fig. 9 (d). The origin of the formation of the natural nanolattice therefore looks similar to those of atomic lattices [10].

3.4 Zeta potential properties

In order to analyze the stability of these nanolattices and prove its formability, we have carried out their zeta potential (ζ) measurements. ζ data are represented in Figure 10 for Ni31, Ni40, Ni44 (TPP only), Ni47 (TOP only) and Ni48 (OA only) samples. The ζ values are respectively 9.6 mV, 12.3 mV, 25 mV, 38.5 mV and 39.3 mV. By convention, particles displaying their $\zeta > 30$ mV are indicative of stable dispersion in ethanol.[10,17] However, this conclusion may not necessarily
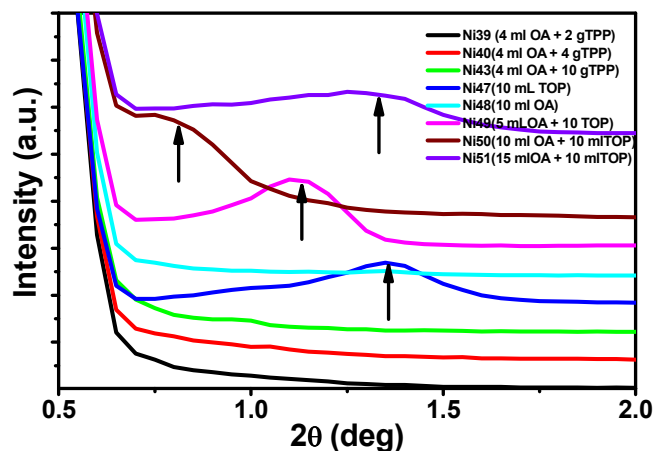
Fig. 8 Grazing indent X-ray diffraction patterns of various samples prepared in different types of surfactants as indicated in the legend. Vertical arrows indicate the GIXRD peaks. Angle of incidence was 0.5° due to which only one peak each is visible.
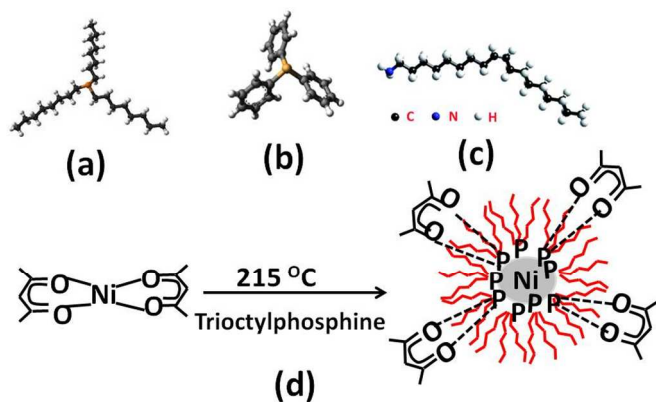
Fig. 9 Structures of (a) trioctylphosphine, $C_{24}H_{51}P$, (b) triphenylphosphine, $C_{18}H_{15}P$ and oleylamine, $C_{18}H_{37}N$ surfactants. (d) Schematic of surfactant or impurity ions attached on the surface of a typical nanoparticle during its preparation.

indicate that the size of these NPs is monodispersed. This has been obvious from their TEM images (fig. 6). In contrast, Ni31, Ni40 and Ni44 samples have their ζ values (9.6 mV, 12.3 mV and 25 mV) less than 30 mV. This may indicate that these NPs are not stably dispersed in ethanol but settles down with time. In other words, they get agglomerated at the bottom of the cubette or the container. This does not however imply that they are agglomerated particles to form nanolattice i.e. ordered self-assembly. This happens only when the particles are formed using TOP as surfactant or one of its component surfactants but not for either TPP or OA, as seen from figs. 7 and 8. If the base-width ($\Delta\zeta$) of the ζ peak is considered, that for TPP only (Ni44) sample has the largest values of all extending from about -75 mV to +100 mV (175 mV). Relatively broader $\Delta\zeta$ of about -10 mV to -50 mV (40 mV) for Ni40 (TPP+OA) sample, of about +18 mV to +55 mV (37 mV) for Ni48 (OA only) sample than about -10 mV to 25 mV (35 mV) for Ni31 (TOP+OA) sample and about +18 mV to +52 mV (34 mV) of Ni48 (TOP only) might indicate that narrower $\Delta\zeta$ favours the
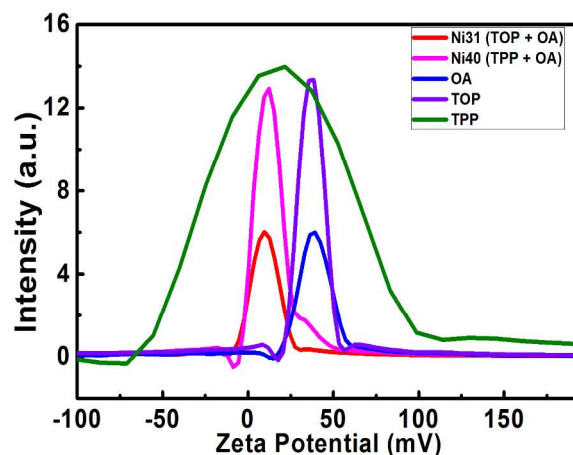
Fig. 10 Zeta potential curves of Ni31, Ni40, Ni44 (TPP only), Ni47 (TOP only) and Ni48 (OA only) samples.

formation of uniform particle size and nanolattice. Therefore, samples made with TPP or OA only are self-assembled (means, agglomerated) partially, yet randomly as usual to form bigger particles, not as nanolattice. The positive/ negative signs of ζ indicate that the particles are positively/ negatively charged in ethanol even though TOP, TPP and OA are non-ionic surfactants. In this, TOP and OA lead to positive signs only. This implies that either these surfactants are dissociated or the impurities if any present in them are dissociated that get interacted with ethanol to give rise to the resultant positive/ negative charge and hence the positive/ negative sign in the ζ values.[10]

3.5 FTIR studies

The ionic state of the NPs observed in the zeta potential data can further be confirmed using their FTIR spectroscopy. They are represented in Figure 11. The peaks near 2958 cm^{-1}, 2923
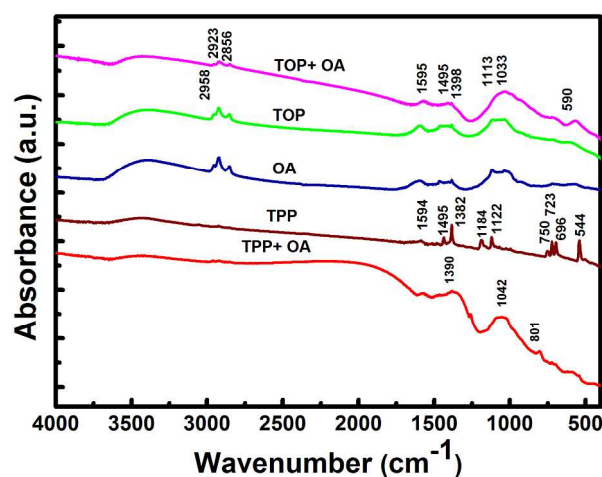
Fig. 10 FTIR of the samples prepared in trioctylphosphine (TOP), triphenylphosphine (TPP) and oleylamine (OA) only, TPP+OA and TOP+OA.

cm^{-1} and 2856 cm^{-1} reveal C-H stretching absorption of TOP, TPP and OAm. These absorption peaks are slightly varied when these surfactants are used separately or in combination of them (cf. ref. [10]). The energy band between 1217 and 910 cm^{-1} are identified as C–P and C-N stretching peaks of TPP, TOP and OAm. Moreover, the absorption band between 1600 cm^{-1} and 1300 cm^{-1} is assigned to the asymmetric in-plane and symmetric rocking mode of terminal methyl group of TOP and OAm. In addition, the peaks near 1595 cm^{-1} and 1033 cm^{-1} have been assigned to the presence of acetylacetonate ligands and C=C bonds of TPP. The other peaks of the TPP only sample are attributed to the various vibrational modes in TPP. Similar attribution is applicable in TPP+OA, TOP only, TOP+OA and OA only samples also. This might indicate that acac ligands are attached to the phosphorus atoms of TOP to form its complex.[10] From these results, it could be confirmed that the TPP, TOP and OAm ligands were successfully capped on the surface of the Ni NPs (fig. 9(d)). Since acac might form complex with P of TOP, their original negative and positive states may remain partially uncompensated after the reduction reaction, complexation and capping. As a result, these –ve/+ve charge pairs might be covered uniformly on the surface of each NP mimicking 'a nucleus and extra nuclear electrons of an atom' and hence each NP forms its (nano)lattice point when several of them were dried together after the preparation and washing. Such a favourable situation however takes place for TOP, not with TPP or OA. It is believed that such favourable situation could be found for many other surfactants that are similar to TOP. Hence, in overall, these results corroborate further the observations of nanolattice formation reported in ref. [10].

4. Conclusions

TOP, TPP and OA as surfactants are responsible for enabling formation of NPs of different types. These surfactants along with acetylacetonate ligands were found from FTIR on the surface of NPs. Due to this, their surface charge states and hence the zeta potential changes accordingly. Random size and spherical shapes were observed for the samples prepared with TPP and OA, and TPP or OA separately, leading to the randomly agglomerated NPs. In contrast, samples formed using TOP only and combination of it with OA naturally exhibited monodispersed particle distribution associated with natural nanolattice without any other external force or surfactants. These results therefore clearly demonstrated the TOP as inducer of monodispersed NPs and hence the lattices of the latter.

Notes and references

[a] UGC-DAE Consortium for Scientific Research, Khandwa Road, Indore (MP) 452001, India.

[b] Department of Physics, ISLE, IPS Academy, Rajendra Nagar, Indore (MP) 452012, India.

[c] Department of Physics, Government Holkar Science College, A. B. Road, Indore (MP) 452001, India.

*Email: okram@csr.res.in, okramgs@gmail.com; Tel: +91-731-2463913

1 J. M. Luther, M. Law, Q. Song, C. L. Perkins, M. C. Beard and A. J. Nozik, *ACS Nano*, 2008, **2**, 271.

2 F. X. Redl, K. S. Cho, C. B. Murray and S. O'Brien, *Nature*, 2003, **423**, 968.

3 S. Sun, C. B. Murray, D. Weller, L. Folks and A. Moser, *Science*, 2000, **287**, 1989.

4 Z. Nie, A. Petukhova and E. Kumacheva, *Nature Nanotech*, 2010, **5**, 15.

5 M. P. Pileni, *J. Phys. Chem.*, 2001, **B105**, 3358.

6 J. Park, E. Kang, S. U. Son, H. M. Park, M. K. Lee, J. ; Kim, K. W. Kim, H. J. Noh, J. H. Park, C. J. Bae, J. G. Park and T. H. Park, *J. Adv. Mater*, 2005, **17**, 429.

7 D. Nykypanchuk, M. M. Maye, D. V. Lelie and O. Gang, *Nature,* 2008, **451**, 549.

8 Y. Min, M. Akbulut, K. Kristiansen, Y. Golan and J. Israelachvili, *Nature Mater*, 2008, **7**, 527.

9 K. J. M. Bishop, C. F. Wimer, S. Soh and B. A. Grzybowski, *Small*, 2009, **5**, 1600.

10 J. Singh, N. Kaurav, N. P. Lalla and G. S. Okram, *J. Mater. Chem. C* 2014, **2**, 8918.

11 S. Carenco, et al., Chem. Mater. 2010, **22**, 1340.

12 Y. T. Jeon, et al. J. Phys. Chem. 2006, **110**, 1187.

13 G. S. Okram, A. Soni and R. Prasad, Adv. Sci. Lett. 2011, **4**, 132.

14 G. S. Okram, et al. *J. Nanosci. Nanotechnol.* 2008, **8**, 4127.

15 A. Roy, et al. J. Appl. Phys. 2004, **96**, 6782.

16 G. Schon and U. Simon, Colloid Polym Sci. 1995, **273**, 101.

17 D. Guo, C. Wu, J. Li, A. Guo, Q. Li, H. Jiang, B. Chen and X. Wang, Nanoscale Res Lett 2009, **4**, 1395.

Faraday Discussions Accepted Manuscript